ACS APPLIED MATERIALS & INTERFACES

Research Article

www.acsami.org

Dual-Enhanced Photocatalytic Activity of Fe-Deposited Titanate Nanotubes Used for Simultaneous Removal of As(III) and As(V)

Wen Liu,[†,‡] Xiao Zhao,[‡] Alistair G. L. Borthwick,[§] Yanqi Wang,[†] and Jinren Ni*[,†]

[†]The Key Laboratory of Water and Sediment Sciences, Ministry of Education, Department of Environmental Engineering, Peking University, Beijing 100871, China

[‡]Environmental Engineering Program, Department of Civil Engineering, Auburn University, Auburn, Alabama 36849, United States

[§]Institute of Energy Systems, School of Engineering, The University of Edinburgh, The King's Buildings, Edinburgh EH9 3JL, United Kingdom

Supporting Information

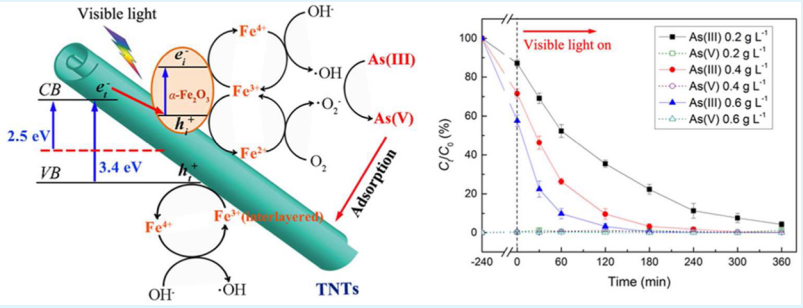

ABSTRACT: Fe-deposited titanate nanotubes (Fe-TNTs) with high photocatalytic activity and adsorptive performance were synthesized through a one-step hydrothermal method. Initial As(III) oxidation followed by As(V) adsorption by Fe-TNTs could simultaneously remove these two toxic pollutants from aqueous solutions. The apparent rate constant value for photo-oxidation of As(III) under UV irradiation by Fe-TNTs was almost 250 times that of unmoidified TNTs. Under visible light, the Fe-TNTs also exhibited enhanced photocatalytic activity after Fe was deposited. Fe^{3+} located in the interlayers of TNTs acted as temporary electron- or hole-trapping sites, and attached α-Fe_2O_3 played the role of a charge carrier for electrons transferred from TNTs. These two effects inhibited electron−hole pair recombination thus promoting photocatalysis. Moreover, the As(V) adsorptive performance of Fe-TNTs also improved, owing to the presence of additional adsorption sites, α-Fe_2O_3, as well as increased pH_{PZC}. Furthermore, Fe-TNTs exhibited good photocatalytic and adsorptive performace even after 5 reuse cycles. The present tests, concerning an initial As(III) photocatalysis and subsequent As(V) adsorption process, highlight the feasibility and importance of Fe used to modify TNTs. This study proposes a feasible method to simultaneously remove As(III) and As(V) from contaminated water using a novel Ti-based nanomaterial.

KEYWORDS: *titanate nanotubes, Fe-deposited, photocatalytic activity, dual-enhanced, visible light, As*

1. INTRODUCTION

TiO_2-devised nanomaterials are increasingly applied as photocatalysts and adsorbents in environmental remediation.[1−4] One-dimensional (1D) nanostructure-based materials are considered promising materials for photocatalytic application.[5,6] Specifically, 1D hydrothermally prepared titanate nanotubes (TNTs) are widely used as heavy-metal adsorbents due to their excellent ion-exchange characteristics, large surface area, and abundant functional groups (−OH).[7−9] However, unlike their precursor, TiO_2, raw TNTs show weak photocatalytic activity due to the rapid recombination of excited electrons and holes after irradiation.[3,10−12] Consequently, there has been a recent upsurge in the number of research studies on the modification of TNTs to enhance their photocatalytic activity. Certain studies focus on the phase transition from titanate to TiO_2 by means of acid or heat treatment,[10,13,14] which can only enhance the photocatalytic activity under UV light, and no studies about response on visible light by calcined or hydrogen TNTs were reported. Others consider deposition of transition or precious metals (e.g., Cu, Pd, W, Au, CdS, etc.) onto TNTs so as to inhibit the recombination of electron−hole pairs by creating a new donor level, which can help to transfer the excited electrons.[15−18] In addition, light adsorption edge to the visible range was also observed after metal deposition.[16,18] Therefore, metal deposition is more energy-efficient and easier to undertake for modification of TNTs than phase transition, especially for low-cost, common metal (like Cu and Fe) deposition.

Received: June 13, 2015
Accepted: August 21, 2015
Published: August 24, 2015

DOI: 10.1021/acsami.5b05263
ACS Appl. Mater. Interfaces 2015, 7, 19726−19735

Arsenic (As) is a highly toxic and carcinogenic pollutant whose presence in the water environment can present a major threat to the ecosystem and human beings through accumulation in the food chain.[19,20] The International Agency for Research on Cancer (IARC) recognizes arsenic and arsenic compounds as group 1 carcinogens, and the EU lists arsenic trioxide, arsenic pentoxide, and arsenate salts as category 1 carcinogens.[21] Two main forms of As are found in water, As(III) and As(V). Of these, As(III) exhibits much higher toxicity than As(V) because of its high affinity to thiols, the active sites of many important enzymes in living bodies.[22] So a common technique for removal of As from aqueous solutions involves oxidation of As(III) to As(V) to reduce toxicity first, followed by further treatment to achieve complete removal.[23,24] Although iron oxides, such as Fe_2O_3 and Fe_3O_4, have been found to be some of the best materials for As removal,[25,26] operational bottlenecks occur due to the oxidation efficiency of As(III) and adsorption capacity of As(III) or As(V). However, the excellent adsorption and photocatalytic characteristics of modified TNTs imply they may play an important role in As removal.[4,27−29] Given the large capacity of Fe oxides for As adsorption, Fe-deposited TNTs with enhanced photocatalytic and adsorptive properties compared with those of TNTs would appear to be a good choice for removing As from aqueous solutions.

In the present study, novel Fe-deposited titanate nanotubes (Fe-TNTs) were synthesized through a one-step hydrothermal method. Both photocatalytic activity and adsorption performance of the Fe-TNTs were greatly enhanced compared to conventional TNTs. The new material was characterized in detail, and the roles of Fe in enhancement of the photocatalytic activity and adsorptive performance were investigated. The main objective is to achieve simultaneous removal of As(III) and As(V) through initial photocatalysis (especially under visible light) and subsequent adsorption using Fe-TNTs. A full discussion is included describing the key role played by Fe as a deposited element in modifying the TNTs used to remove As(III) and As(V).

2. EXPERIMENTAL SECTION

2.1. Chemicals. All chemicals were of analytical grade and did not require further purification. TiO_2 nanoparticles (P25, 80% anatase and 20% rutile) were purchased from Degussa Corporation of Germany. $FeCl_3{\cdot}6H_2O$, NaOH, and absolute ethanol (also used to synthesize Fe-TNTs) were obtained from Tianjin Fuchen Chemical Company, China. High-purity deionized (DI) water (Millipore Co., 18.2 MΩ cm) was used to prepare all solutions. $NaAsO_2$ and $Na_2HAsO_4{\cdot}7H_2O$ (Sigma-Aldrich Co.) were, respectively, used to prepare As(III) and As(V) stock solutions (each 100 mg L^{-1}).

2.2. Synthesis of Fe-TNTs. A modified one-step water−ethanol hydrothermal method was used to fabricate Fe-TNTs. First, 1.08 g of $FeCl_3{\cdot}6H_2O$ and 0.48 g of NaOH were mixed in a beaker with 40 mL of absolute ethanol. After stirring under ultrasonic conditions for 30 min, 0.6 g of TiO_2 (P25), 21 g of NaOH, and 25 mL of deionized water were further added. The mixture was then stirred for a further 30 min under ultrasonic conditions, transferred into a Teflon reactor with stainless steel coating, and heated at 150 °C for 24 h. Finally, the precipitates were washed with deionized water to neutral, and Fe-TNTs were obtained after drying at 80 °C for 6 h.

For comparison purposes, conventional TNTs were also synthesized through the traditional hydrothermal method described in our previous studies.[7,30] Typically, 1.2 g of TiO_2 (P25) and 29 g of NaOH were mixed and dispersed into 66 mL of deionized water. After the mixture was heated in a Teflon reactor at 130 °C for 72 h, the products were washed to neutral and dried at 80 °C.

2.3. Photocatalytic Reactions. Photocatalytic experiments were carried out in a quartz reactor (300 mL total volume) (Figure S1 in the Supporting Information), and a metallic cover was placed outside to isolate other light sources. A 100 mL portion of As(III) solution with an initial concentration of 10 mg L^{-1} was added into the quartz reactor. After the solution pH was adjusted to 3.0 using dilute HCl and NaOH solution, 0.02−0.06 g of Fe-TNTs were mixed. Before photocatalytic reaction, the mixture was stirred in the dark for 4 h to reach equilibrium for As(III) adsorption onto Fe-TNTs. Afterward, a 150 W mercury lamp (365 nm, 2.5 mW cm^{-2}, Beijing Electric Light Sources Research Institute, China) was switched on to start the photocatalysis reaction. During the photocatalysis process, cooling air was poured in from the top so as to maintain the reaction system at a constant temperature (25 ± 2 °C). Samples were taken every 10 min, immediately centrifuged at 10 000 rpm for 2 min, and filtered using a 0.22 μm membrane. Photolysis experiments without addition of Fe-TNTs were also conducted as control tests. Each set of experiments was performed in triplicate.

The As(III) photocatalytic reactions are expressed by the classical Langmuir−Hinshelwood (L−H) model[29]

$$-\frac{dC_t}{dt} = r = k_r\frac{K_L C_t}{1 + K_L C_t} \quad (1)$$

where C_t (mg L^{-1}) is the As(III) concentration at time t (min), r (mg L^{-1} min^{-1}) is the photocatalytic reaction rate, k_r (mg L^{-1} min^{-1}) is the photocatalytic reaction rate constant, and K_L (L mg^{-1}) is the Langmuir constant of adsorption. We consider the simplified first-order kinetic model

$$\ln(C_0/C_t) = k_1 t \quad (2)$$

where C_0 (mg L^{-1}) is the initial concentration of As(III), and k_1 (min^{-1}) represents the apparent rate constant of reaction ($k_1 = k_r K_L$).

To investigate the removal of As(III) and As(V), experiments were first carried out on the adsorption of these two As ions under different pH values. A 50 mL portion of As solution with an initial concentration of 10 mg L^{-1} was added into an Erlenmeyer flask. After the solution pH was adjusted in the range from 1 to 9, 0.01 g Fe-TNTs was added and the mixture shaken (25 °C, 200 rpm) for 6 h. Samples were taken before and after adsorption, and the As concentration was immediately measured using atomic fluorescence spectroscopy (AFS-9130, Beijing Jitian, China) after centrifugation and filtration. The adsorption capacity (Q_e, mg g^{-1}) and removal efficiency (R, %) of As at equilibrium are calculated from

$$Q_e = \frac{(C_0 - C_e)V}{m} \quad (3)$$

and

$$R = \frac{(C_0 - C_e)}{C_0} \times 100\% \quad (4)$$

where C_0 (mg L^{-1}) is the initial As concentration, C_e (mg L^{-1}) is the equilibrium As concentration, V (mL) is the solution volume, and m (g) is the mass of Fe-TNTs.

Photocatalysis experiments at conditions close to real conditions were then carried out under visible light irradiation. A 10 mg L^{-1} As(III) solution was added into a quartz reactor at pH 3.0. After addition of 0.02−0.06 g Fe-TNTs and an initial 4 h stirring in the dark, a 500 W xenon arc lamp (470 nm, Beijing Electric Light Sources Research Institute, China), which was used in conjunction with UV cutting filter ($\lambda \geq 420$ nm), was switched on as the visible light source to start the photocatalysis reaction. Also, the same conditions and procedures were conducted as the aforementioned photocatalysis experiments, except for the light source. Samples were collected at specific intervals and immediately measured. Control experiments were also conducted without addition of Fe-TNTs.

2.4. Reuse of Fe-TNTs. To evaluate the application potential of Fe-TNTs for removal of As(III) and As(V), the material was reused after photocatalysis−adsorption experiments under visible light.

DOI: 10.1021/acsami.5b05263
ACS Appl. Mater. Interfaces 2015, 7, 19726−19735

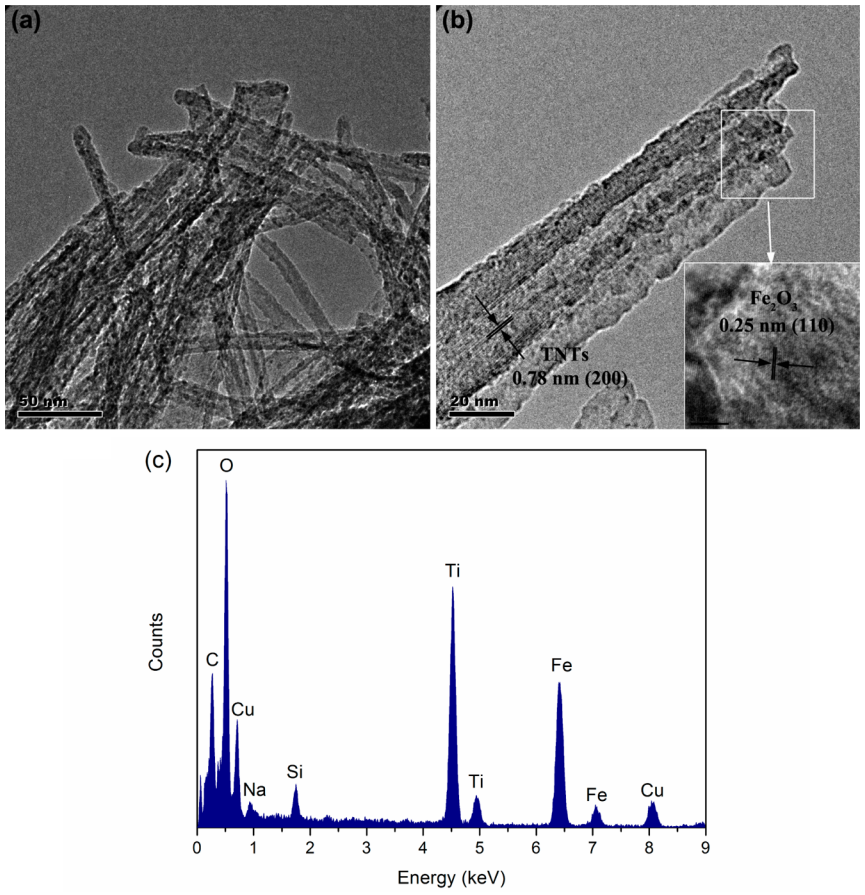

Figure 1. (a) TEM, (b) HRTEM image, and (c) EDS spectrum of Fe-TNTs.

Especially, a photocatalysis−adsorption test was carried out first with initial As(III) concentration of 10 mg L^{-1} and Fe-TNTs dosage of 0.6 g L^{-1} at pH 3.0. After an initial 240 min of adsorption in the dark and a subsequent 180 min of photocatalysis under visible irradiation, materials were separated by centrifugation and filtration. Afterward, the materials were immersed into 100 mL of 1.0 mol L^{-1} NaOH solution and shaken for 4 h to desorb As(V). After desorption, Fe-TNTs were washed to neutral using DI water, and then reused to remove As under the same conditions via photocatalysis and adsorption. Reuse of Fe-TNTs lasted for 5 cycles. In addition, the concentration of Fe dissolved into solution in each cycle was detected on an inductively coupled plasma−optical emission spectrometry (ICP-OES, Prodigy, Leeman).

2.5. Analysis of Hydroxyl Radicals. Formation of hydroxyl radicals ($^{\bullet}OH$) in the photocatalysis reaction was detected by a photoluminescence (PL) technique using terephthalic acid as the probe molecule. Terephthalic acid reacted readily with $^{\bullet}OH$ to form a highly fluorescent product, 2-hydroxyterephthalic acid, whose intensity was proportional to the amount of $^{\bullet}OH$ present. A total of 0.01 g of Fe-TNTs was dispersed into a mixture of 0.5 mmol terephthalic acid and 2 mmol NaOH occupying a total volume of 10 mL in a dish. Afterward, the mixture was irradiated under UV light, and samples were taken every 15 min. After filtration, the PL spectra of samples were measured by a Hitachi F-4500 fluorescence spectrophotometer with photomultiplier tube (PMT) R928. The PL intensity of 2-hydroxyterephthalic acid was determined at 425 nm, excited by 320 nm light.

2.6. Characterizations. Morphology of the material was analyzed using a Tecnai30 FEG transmission electron microscopy microscope (TEM, FEI) operating at 300 kV. Energy dispersive X-ray spectra (EDS) were also recorded. The crystal phase of the sample was obtained by means of a Dmax/2400 X-ray diffractometer (XRD, Rigaku, Japan) using Cu Kα radiation (λ = 1.5418 Å) at a scan rate (2θ) of 4°/min. Specific surface areas of the materials were determined via nitrogen adsorption−desorption isotherms at −196 °C using an ASAP2010 adsorption apparatus (Micromeritics) based on Brunauer-Emmett-Teller (BET) theory. Pore volume and mean pore diameter were measured by means of the nitrogen adsorption volume at a relative pressure of 0.99. Surface functional groups were determined using Fourier transform infrared spectroscopy (FTIR, Tensor 27, Bruker, Germany) through the KBr pellet method. Element composition and the oxidation states of samples were recorded on an AXIS-Ultra X-ray photoelectron spectroscopy (XPS, Kratos, England) using Al Kα X-ray source at 15 kV and 15 mA. The standard C 1s peak (Binding energy, E_b = 284.80 eV) was used to eliminate static charge effects. The UV−vis spectrum of each sample was recorded by a UV-1800 instrument (Shimadzu, Japan) after the material was dispersed in water. Diffuse reflectance (DRS) UV−vis adsorption spectra of the materials were obtained using a UV-2400 spectrophotometer (Shimadzu, Japan). $BaSO_4$ powder was used as reference at all energies (100% reflectance), and reflectance measurements were converted to adsorption spectra using the Kubelka−Munk function. Zeta potential and size of samples were obtained using a Nano-ZS90 Zetasizer (Malvern Instruments).

3. RESULTS AND DISCUSSION

3.1. Characteristics of Fe-TNTs. The as-synthesized TNTs comprised 4−5 layers of hollow and open-ended nanotubes, which had uniform interior (ca. 4.5 nm) and outer (ca. 9 nm) diameters (Figure S2 in the Supporting Information). The interlayer distance was 0.75 nm (Figure S2b in the Supporting Information).[30] EDS analysis indicated that the main elements in TNTs were Na, O, and Ti (Figure S2c in the Supporting Information). After the Fe was deposited, the surface of nanotubes became rough, with some nanoparticles attached

DOI: 10.1021/acsami.5b05263
ACS Appl. Mater. Interfaces 2015, 7, 19726−19735

(Figure 1). The interlayer distance of Fe-TNTs increased to 0.78 nm due to entry of Fe^{3+}.[7] The lattice distance of attached nanoparticles was 0.25 nm (Figure 1b), which was assigned to the (110) plane of Fe_2O_3 (JCPDS 24-0072). An Fe element peak was also observed in the results from EDS analysis (Figure 1c), indicating that Fe had been successfully deposited onto TNTs.

XRD further confirmed the deposition of Fe (Figure 2). Diffraction peaks at $2\theta \approx 10°$, 24°, 28°, 48°, and 62° were all

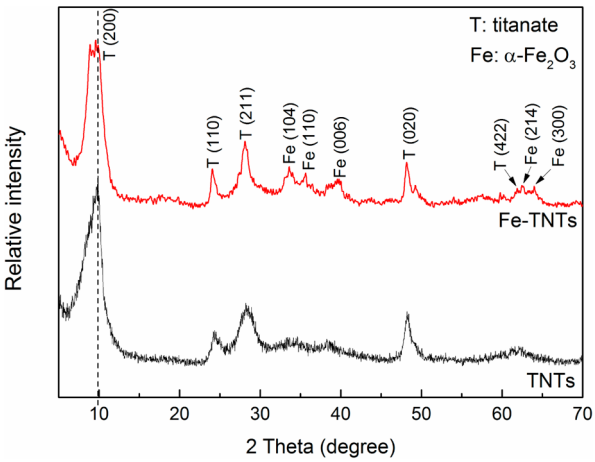

Figure 2. XRD patterns of TNTs and Fe-TNTs.

attributed to TNTs, and in particular, the 10° peak represented the interlayer space of TNTs.[31,32] For Fe-TNTs, besides the diffraction of TNTs, the new peaks at 2θ = 33.6°, 35.6°, 40.0°, 44.7°, 62.5°, and 64.0° were consistent with (104), (110), (006), (202), (214), and (300) planes of α-Fe_2O_3 phases (JCPDS 24-0072). Moreover, the interlayer peak of Fe-TNTs shifted to 9.59° from 9.86° of TNTs, indicating an increase in the interlayer distance (smaller 2θ degree meant larger interlayer distance), related to the entry of Fe^{3+}. Here, the TNTs were a kind of sodium trititanate with the chemical formula $Na_xH_{2-x}Ti_3O_7$ (x = 0–0.75, depending on remaining sodium ions), which was composed of edge-sharing $[TiO_6]$ octahedra as the basic skeleton and H^+/Na^+ between the layers.[31−33] Interlayer H^+/Na^+ ions were readily replaced by Fe^{3+} during the hydrothermal process, causing the interlayer distance to increase. Deposited Fe in Fe-TNTs therefore existed in two forms: α-Fe_2O_3 attached on TNTs, and Fe^{3+} located in the interlayers of TNTs.

Figure 3 shows the FTIR spectra obtained for the both the TNTs and Fe-TNTs. Considering the spectrum related to the TNTs, the bands at 476 and 925 cm^{-1} corresponded, respectively, to vibration of the $[TiO_6]$ octahedron and four-coordinate Ti−O stretching.[32,34] After Fe deposition, an additional band appeared at 652 cm^{-1} representing Fe−O vibration.[35] Bands at 3313 and 1631 cm^{-1} were ascribed to the stretching vibrations of O−H and H−O−H, respectively. The shift of the O−H band to 3395 cm^{-1} for Fe-TNTs was due to the interaction of hydroxyl groups with Fe^{3+}.[34] The band at 1383 cm^{-1} corresponding to O−Na stretching vibration almost disappeared for Fe-TNTs, confirming that the interlayered Na^+ ions were exchanged by Fe^{3+}.[36]

Table 1 provides a list of key physiochemical parameters describing the unmodified TNTs and Fe-TNTs. The large BET surface area (162.8 m^2 g^{-1}) and single point total pore volume (0.38 cm^3 g^{-1}) of the Fe-TNTs benefited both photocatalysis

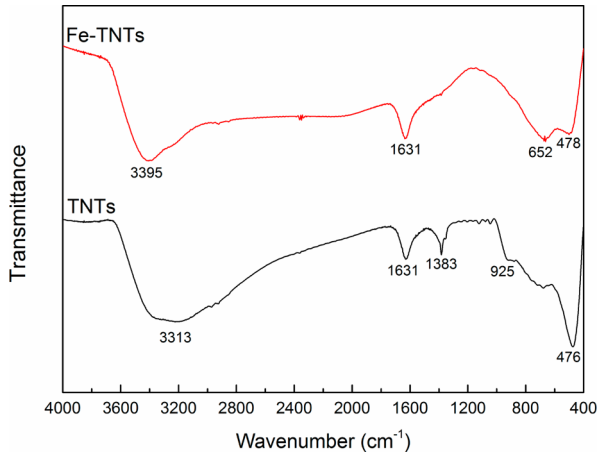

Figure 3. FT-IR spectra of TNTs and Fe-TNTs.

and adsorption through enhanced contact with As ions. Moreover, the N_2 adsorption−desorption isotherms on Fe-TNTs fitted type IV isotherms with H3 hysteresis loops according to BDDT classification,[37] suggesting the presence of mesopores (2−50 nm) in Fe-TNTs (Figure S3a in the Supporting Information). The pore size of Fe-TNTs exhibited a trimodal distribution, as shown in Figure S3b in the Supporting Information. Pores with peak diameters in the ranges 3−4, 8−9, and 10−20 nm were, respectively, attributed to the interior of the nanotubes, gaps between the Fe_2O_3 nanoparticles and TNTs, and voids in the aggregation of the nanotubes.[38,39] Attachment of Fe_2O_3 nanoparticles inevitably blocked some pores of the TNTs, leading to a decrease in specific surface area and pore volume compared to the unmodified TNTs. The point of zero charge (pH_{PZC}) for Fe-TNTs increased to 5.49 after Fe was deposited, a much higher value than that for unmodified TNTs (2.56) (Figure S4 in the Supporting Information), which is attributed to the adsorption of metal anions, such as As(V).[27,28]

3.2. Adsorption of As(III) and As(V) by Fe-TNTs. Figure 4 depicts the adsorption of As(III) and As(V) for different pH values. The adsorption capacity of As(III) on TNTs remained small (<10 mg g^{-1}) throughout the range of pH considered, and was related to the form of As(III) species in solution. Molecular H_3AsO_3 was the main species of As(III) over a wide pH range (Figure S5a in the Supporting Information), and complexation by hydroxyl groups of Fe-TNTs was the dominant mechanism,[27] resulting in an almost unchanged As(III) adsorption capacity. Photocatalysis was therefore necessary to remove As(III), after which the oxidation products, As(V), could be further adsorbed onto Fe-TNTs.

The adsorption was extremely different for As(V) adsorption onto Fe-TNTs as a function of pH. Fe-TNTs exhibited good adsorption performance for As(V), especially at low pH (2 and 3). For instance, the adsorption capacity of As(V) reached 49.1 mg g^{-1} at pH 3, with a correspondingly high removal efficiency of 98.2%. Fe-TNTs were positively charged at low pH (Figure S4 in the Supporting Information), and thus could capture As(V) anions ($H_2AsO_4^-$) through electrostatic attraction (Figure S5b in the Supporting Information). Moreover, As(V) in the main form of molecular H_3AsO_4 was hardly attracted to Fe-TNTs at pH 1, even though the Fe-TNTs had their highest positive charge at low pH. As the pH further increased (>3), the amount of positive charge decreased (Figure S4 in the Supporting Information), thus lowering the

DOI: 10.1021/acsami.5b05263
ACS Appl. Mater. Interfaces 2015, 7, 19726−19735

Table 1. Physicochemical Parameters of Unmodified TNTs and Fe-TNTs

material	BET surface area (m^2 g^{-1})	single point total pore volume (cm^3 g^{-1})	av pore diameter (nm)	pH_{PZC}	atomic percentage content (%)			
					Na	O	Ti	Fe
Fe-TNTs	162.8	0.38	9.3	5.49	9.1	62.7	21.8	6.4
TNTs	272.3	1.26	18.5	2.56	12.3	64.3	23.4	0.0

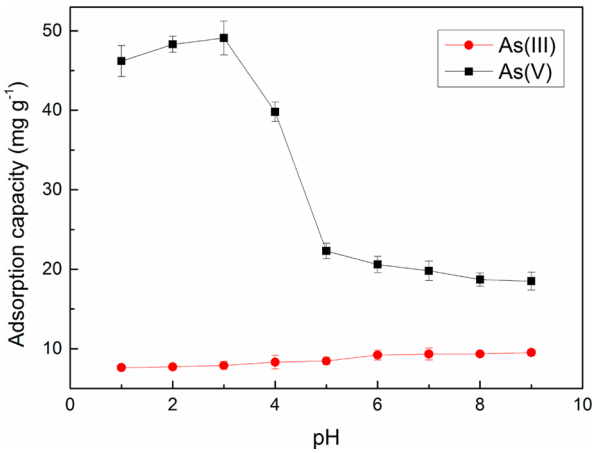

Figure 4. Adsorption of As(III) and As(V) by Fe-TNTs at different pH. (Initial As concentration = 10 mg L^{-1}; Fe-TNTs dosage = 0.2 g L^{-1}.)

As(V) adsorption capacity. Moreover, increased OH^- at higher pH would compete for adsorption sites with As(V) anions, further lowering the adsorption capacity.[27,28,34] Noting the high adsorption efficiency of As(V), a pH value of 3 was chosen for the following photocatalysis–adsorption experiments.

3.3. Photocatalysis of As(III) by Fe-TNTs under UV Light. Figure 5 presents time histories of As(III) and As(V)

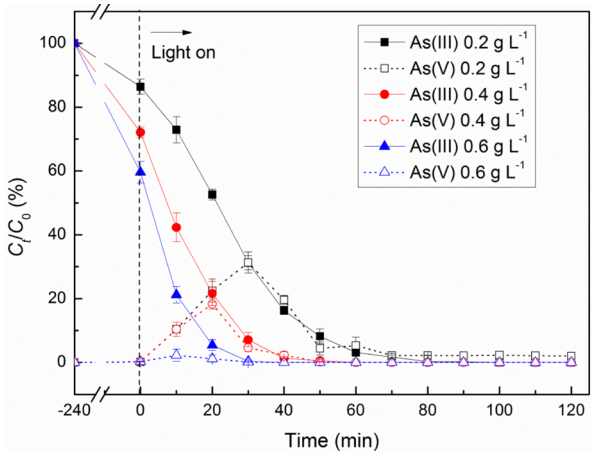

Figure 5. Photocatalysis–adsorption of As(III) and As(V) by Fe-TNTs at different initial dosages under UV light. (Initial As(III) concentration = 10 mg L^{-1}; solution pH = 3.0.)

concentrations, each for three initial dosage values, throughout the photocatalysis–adsorption process under UV light. Before the light was switched on (from t = −240 to 0 min), a portion of As(III) was removed in the dark by adsorption on the Fe-TNTs. During this phase, the adsorption capacity of As(III) onto Fe-TNTs was limited, given that there was still 59.6% As(III) remaining even at a high Fe-TNTs dosage of 0.6 g L^{-1}. In addition, adsorption of As(III) could reach equilibrium with 180 min (Figure S6 in the Supporting Information), so 240 min is enough for As(III) adsorption in this study. Once the light was switched on, the removal of As(III) was primarily due to photocatalysis (for t = 0 to 120 min), and the total removal efficiency exceeded 99% after 70 min for all three initial dosages considered. Notably, 99.6% of As(III) of initial dosage 0.6 g L^{-1} was photo-oxidized within 30 min, indicating the extremely high photocatalytic ability of Fe-TNTs. Table 2 lists the

Table 2. Parameters of First-Order Kinetic Model for As(III) Photocatalysis by Fe-TNTs

dosage (g L^{-1})	UV light		vis light	
	k_1 (min^{-1})	R^2	k_1 (min^{-1})	R^2
0.2	0.0596	0.9195	0.0086	0.9965
0.4	0.0917	0.9506	0.0173	0.9915
0.6	0.1512	0.9356	0.0263	0.9886

parameters of the first-order kinetic model for As(III) under photocatalysis by Fe-TNTs. The higher the initial dosage of Fe-TNTs is, the larger the value of the apparent rate constant (k_1) is. Very weak photocatalytic performance for As(III) oxidation was found for TNTs (Figure S7 in the Supporting Information). Comparatively, the k_1 value for photo-oxidation of As(III) by Fe-TNTs (0.1512 min^{-1}) was almost 250 times that of unmodified TNTs (0.0006 min^{-1}) at the same initial dosage of 0.6 g L^{-1}, suggesting Fe played an important role and Fe deposition substantially enhanced the photocatalytic activity of TNTs.

For As(V) removal, the ratio C_t/C_0 in Figure 5 is equivalent to the conversion efficiency from As(III) to As(V), as the value of C_0 was 10 mg L^{-1} (if total conversion). The process involved simultaneous production and elimination of As(V). On one hand, As(III) was photo-oxidized to As(V) which then accumulated in solution. On the other hand, the produced As(V) was continuously adsorbed onto Fe-TNTs, and Figure S6 in the Supporting Information indicates that adsorption of As(V) could reach to equilibrium within 300 min while it mainly occurred in the first 90 min. Therefore, the As(V) concentration initially increased to a peak value before declining to about zero. At high (0.6 g L^{-1}) initial dosage Fe-TNTs almost no As(V) was detected over the entire photocatalysis–adsorption process, indicating that the abundant adsorption sites simultaneously adsorbed all the produced As(V). Therefore, a combination of photocatalysis and adsorption on Fe-TNTs led to the efficient removal of As(III) and As(V), thus achieving the goal of complete removal of As.

3.4. Removal of As(III) and As(V) by Fe-TNTs under Visible Light. Figure 6 shows results corresponding to those in Figure 5, except that visible light is used instead of UV as the light source. From the time histories in Figure 6, it can be seen that As(III) was also efficiently oxidized to As(V) under visible light, although the photocatalytic reactions required more time than those under UV irradiation (Figure 5). The removal efficiency of As(III) reached 99.6% at 300 min for an initial dosage of 0.4 g L^{-1} Fe-TNTs and 99.5% at 180 min for an

DOI: 10.1021/acsami.5b05263
ACS Appl. Mater. Interfaces 2015, 7, 19726–19735

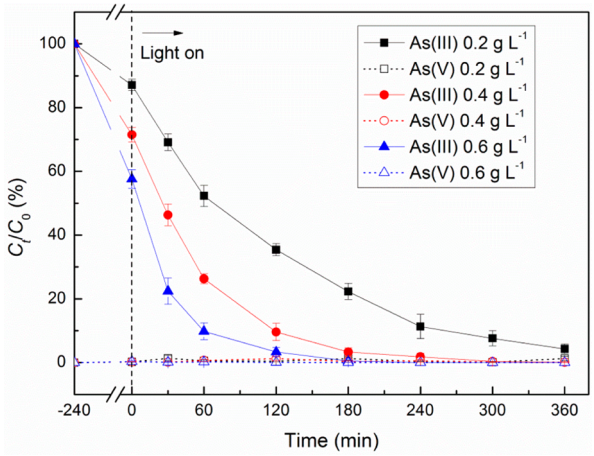

Figure 6. Photocatalysis–adsorption of As(III) and As(V) by Fe-TNTs at different initial dosages under visible light (initial As(III) concentration = 10 mg L^{-1}; solution pH = 3.0).

initial dosage of 0.6 g L^{-1} Fe-TNTs, indicating good photocatalytic performance even under visible light. Although some As(III) converted to As(V) through photolysis and photocatalysis by unmodified TNTs (Figure S8 in the Supporting Information), the conversion efficiency was relatively low (8.0% and 9.6%, respectively, within 360 min). This indicates that oxidation of As(III) under visible light was greatly enhanced by Fe-TNTs due to Fe deposition, and the mechanism will be discussed later in detail. Furthermore, only trace amounts of As(V) accumulated in solution (<2%) over the entire photocatalysis–adsorption process. The photocatalytic rate of As(III) oxidation decreased after UV light was replaced by visible light, but the adsorption rate of As(V) was unaffected, resulting in immediate uptake of As(V). The high photocatalytic activity of Fe-TNTs under visible light is of great importance for future applications in environmental remediation. Considering the excellent removal efficiency of As(III) and As(V) at 0.6 g L^{-1} of Fe-TNTs, this optimum dosage was chosen for the further reusability tests.

3.5. Enhancement Mechanisms of Photocatalytic Activity and Adsorptive Property. *3.5.1. Role of Deposited Fe on Enhancement of Photocatalytic Activity.* The preceding results show that the photocatalytic activity of TNTs was greatly enhanced by deposited Fe. For TNTs, the electron–hole pairs easily recombined after excitation through irradiation, leading to extremely low photocatalytic activity.[3,10] The deposited Fe existed in two forms in Fe-TNTs, i.e., interlayered Fe^{3+} and α-Fe_2O_3, resulting in dual enhancement of photocatalytic activity. First, the Fe^{3+} in the interlayers of TNTs could act as a temporary electron (e^-)- or hole (h^+)-trapping site that inhibited recombination,[40] through the following processes:

$$\text{Fe-TNTs} + h\nu \rightarrow e_t^- + h_t^+ \quad (5)$$

$$Fe^{3+} + e_t^- \rightarrow Fe^{2+} \text{ (electron trap)} \quad (6)$$

$$Fe^{3+} + h_t^- \rightarrow Fe^{4+} \text{ (hole trap)} \quad (7)$$

Due to the instability of Fe^{2+} and Fe^{4+}, transfer of trapped charges from Fe^{4+} and Fe^{2+} to Fe^{3+} also occurred in the titanate surface as follows:

$$Fe^{2+} + Ti^{4+} \rightarrow Fe^{3+} + Ti^{3+} \text{ (electron transfer)} \quad (8)$$

$$Fe^{4+} + OH^- \rightarrow Fe^{3+} + {}^{\bullet}OH \text{ (hole transfer)} \quad (9)$$

Second, α-Fe_2O_3 could also generate an electron–hole pair under irradiation, and therefore act as a charge carrier for electrons transferred from TNTs. The TEM and XRD analyses showed the close coupling between TNTs and α-Fe_2O_3, which meant that an excited electron from TNTs with a lower conduction band could recombine with a hole in Fe_2O_3, thus inhibiting recombination of electron–hole pairs of TNTs.[41] The processes are summarized as follows:

$$\text{Fe-TNTs} + h\nu \rightarrow e_t^- + h_t^+ \quad (10)$$

$$Fe_2O_3 + h\nu \rightarrow e_t^- + h_t^+ \quad (11)$$

$$Fe^{3+} + e_t^- \rightarrow Fe^{2+} \quad (12)$$

$$Fe^{2+} + O_2 \rightarrow Fe^{3+} + {}^{\bullet}O_2^- \quad (13)$$

$$Fe^{3+} + h_t^+ \rightarrow Fe^{4+} \quad (14)$$

$$Fe^{4+} + OH^- \rightarrow Fe^{3+} + {}^{\bullet}OH \quad (15)$$

During photocatalysis, As(III) oxidation involved the following reactions:[42]

$$As(III) + {}^{\bullet}OH \rightarrow As(IV) + OH^- \quad (16)$$

$$As(III) + {}^{\bullet}O_2^- + 2H^+ \rightarrow As(IV) + H_2O_2 \quad (17)$$

$$As(IV) + O_2 \rightarrow As(V) + {}^{\bullet}O_2^- \quad (18)$$

$$As(III) + H_2O_2 \rightarrow As(V) + 2OH^- \quad (19)$$

As illustrated by the UV–vis spectra (DRS) (Figure 7), the TNTs exhibited an adsorption edge of 361 nm, whereas Fe

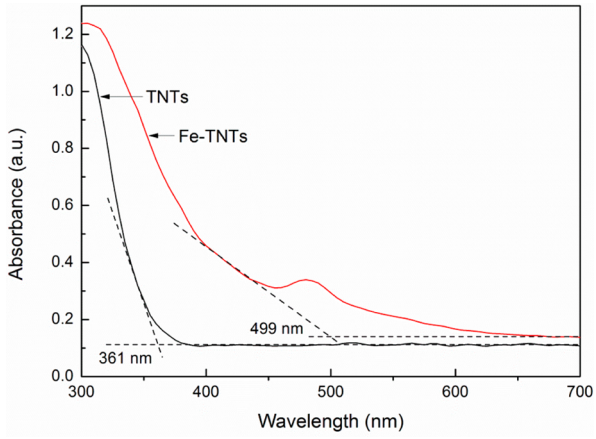

Figure 7. UV–vis spectra (DRS) of TNTs and Fe-TNTs.

deposition led to a dramatic red shift into the visible range of 499 nm. For Fe-TNTs, the peak at ca. 480 nm was related to intrinsic absorption of Fe(III). Using the Kubelka–Munk method,[43] the band gap energy (E_g) of the Fe-TNTs was determined as 2.5 eV, a much lower value than that of the unmodified TNTs (3.4 eV). After Fe was deposited, the Fe 3d electron energy levels were higher than those of Ti 3d, leading to the levels emerging in the gap region between the O 2p and Ti 3d dominant bands.[44] The red shift to visible region in the UV–vis spectra (DRS) of Fe-TNT implies this is a promising candidate for solar energy applications under visible light, as

DOI: 10.1021/acsami.5b05263
ACS Appl. Mater. Interfaces 2015, 7, 19726–19735

confirmed in Figure 6. Although previous studies confirmed the calcination and acid treatment can enhance the photocatalytic activity of TNTs under UV light, no visible light can be adsorbed and used by these TNTs materials (calcined and hydrogen TNTs) for photocatalysis.[4,10,13,14]

PL spectra of terephthalic acid reflected the formation of •OH under UV irradiation in the presence of Fe-TNTs (Figure 8). It can be seen that the fluorescence intensity amplified with

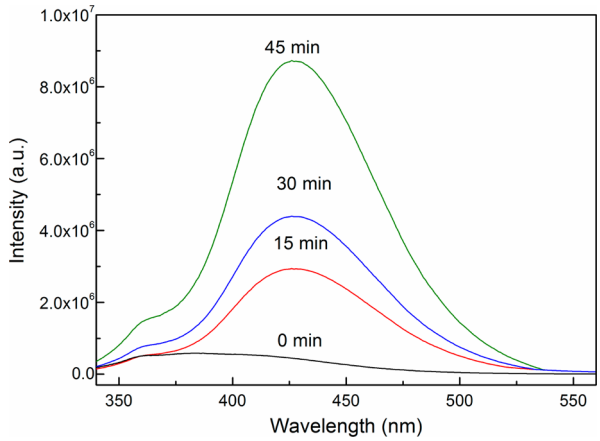

Figure 8. PL spectra for terephthalic acid in the presence of Fe-TNTs as a function of irradiation time.

increasing irradiation time, indicating growth in the amount of •OH in the presence of Fe-TNTs. However, almost no •OH formed when TNTs were used as the photocatalyst (Figure S9 in the Supporting Information), again implying that Fe deposition greatly enhanced photocatalytic activity.

3.5.2. Role of Deposited Fe on Enhancement of Adsorptive Property. Fe-TNTs also exhibited an excellent adsorptive property for As(V). According to the two-site Langmuir isotherm model (Supporting Information), the maximum adsorption capacity of As(V) on Fe-TNTs was found to be 88.72 mg g^{-1}, a much larger value than that for the unmodified TNTs of 27.54 mg g^{-1} (Table S1 in the Supporting Information). Two contributory reasons for this enhancement of the adsorptive property are the following: (1) there is an increase in the pH_{PZC}-induced efficient capture of As(V) anions through electrostatic attraction, and (2) the deposited α-Fe_2O_3 could also adsorb As(V) though surface hydroxyl groups. It is relevant to note the two kinds of adsorption sites in Fe-TNTs, i.e., TNTs and α-Fe_2O_3 (Supporting Information). Therefore, the critical problem of small adsorption capacity of TNTs for the metal anion, As(V), is also solved by Fe-TNTs due to Fe deposition, which is the basis for simultaneous removal of both As(III) and As(V).

The adsorption process of As(V) comprised initial electrostatic attraction and subsequent complexation. This is further illustrated by the results of the XPS analysis in Figure 9, which showed that the main component elements of TNTs were Na, O, and Ti (Figure 9a). After the Fe was deposited, the Fe 3d peak emerged, and the atomic percentage of Fe on Fe-TNTs was 6.4% (Table 1), in accordance with the EDS spectra (Figure 1c). The atomic percentage of Na in Fe-TNTs decreased to 9.1% compared to 12.3% in TNTs, owing to the ion-exchange of Fe^{3+} with Na^+ in the interlayers. An As 3d peak appeared after adsorption, indicating the successful combination of As(V) by Fe-TNTs. Figure 9b shows a high-resolution spectral view in the vicinity of O 1s; the peaks at ca. 532 and 530 eV were, respectively, attributed to O bonded with metals (Me−O) and from hydroxyl groups (−OH).[45] The composition percentage of −OH for Fe-TNTs (20.9%) was higher than that for TNTs (5.6%), due to the presence of large hydroxyl groups attached to the α-Fe_2O_3 surface. It has previously been established that −OH groups play a major role in As(V) adsorption, with complexation the adsorption mechanism.[46−48] Figure S10 in the Supporting Information illustrates the difference between the two main complexation processes: bidentate complexation does not introduce −OH groups whereas monodentate complexation replaces a single −OH by two −OH groups from As(V). For adsorption of As(V) by Fe-TNTs, the −OH percent further increased to 32.5% after adsorption, suggesting that monodentate complexation of As(V) must have occurred in the adsorption process. The peaks at ca. 711 and 725 eV in the high-resolution profile of Fe corresponded to 2p 3/2 and 2p 1/2 of oxidized iron (Figure 9c).[49,50] In particular, the 2p 3/2 peak related to Fe(III) from α-Fe_2O_3 (ca. 711 eV) and located in the interlayers (Ti−O−Fe, ca. 713 eV).[49] The slight decrease in amplitude of Ti−O−Fe peak after adsorption was due to H^+ replacing part of the interlayered Fe^{3+} under acid conditions (pH 3 for the adsorption experiment). The high-resolution view shows that the adsorbed As was entirely composed of As(V) (Figure 9d), suggesting full conversion of As(III) during photocatalysis.

3.5.3. Mechanisms for Simultaneous Photocatalysis of As(III) and Adsorption of As(V) by Fe-TNTs. Figure 10 depicts schematically the photocatalysis and adsorption processes for co-removal of As(III) and As(V) by Fe-TNTs. Deposited Fe greatly increases the photocatalytic activity of TNTs, leading to a dual-enhancement effect on arsenic removal. The interlayered Fe^{3+} acts as a temporary electron- or hole-trapping site, while loaded α-Fe_2O_3 helps transfer electrons created by the TNTs, both mechanisms of which inhibit the electron−hole pair recombination of TNTs. In addition, reactive oxygen species (•OH and $•O_2^-$) form during the conversion process of Fe^{4+}/Fe^{2+} to Fe^{3+}, which then oxidize As(III) to As(V). Afterward, As(V) can be efficiently adsorbed onto Fe-TNTs through complexation.

In conclusion, Fe is an ideal element by which to modify TNTs so as to achieve simultaneous removal of As(III) and As(V). The synthesized Fe-TNTs are different from the conventional sodium and hydrogen TNTs considering its powerful properties on photocatalysis and adsorption. On one hand, deposition of Fe significantly enhances photocatalytic performance, especially under visible light. On the other hand, deposited iron oxide has excellent adsorptive characteristics and so is ideal for As(V) removal. A practicable technology for arsenic removal is first to modify TNTs using Fe via a one-step hydrothermal method, and then to use the synthesized Fe-TNTs to remove simultaneously As(III) and As(V) through a photocatalysis−adsorption process.

3.6. Reuse of Fe-TNTs for As(III) and As(V) Removal. Fe-TNTs was reused after desorption for removal of As(III) and As(V) under visible light via 5 cycles (Figure 11). The desorption rate of As(V) from Fe-TNTs was >99% in each cycle with 1.0 mol L^{-1} NaOH solution treatment. It is found that, even after 5 continuous photocatalysis−adsorption cycles, the final removal efficiency of As(III) and As(V) could reach up to 97.8% and 99.8%, respectively, suggesting good reusability of Fe-TNTs. Moreover, only a total amount of 4.3% of Fe

DOI: 10.1021/acsami.5b05263
ACS Appl. Mater. Interfaces 2015, 7, 19726−19735

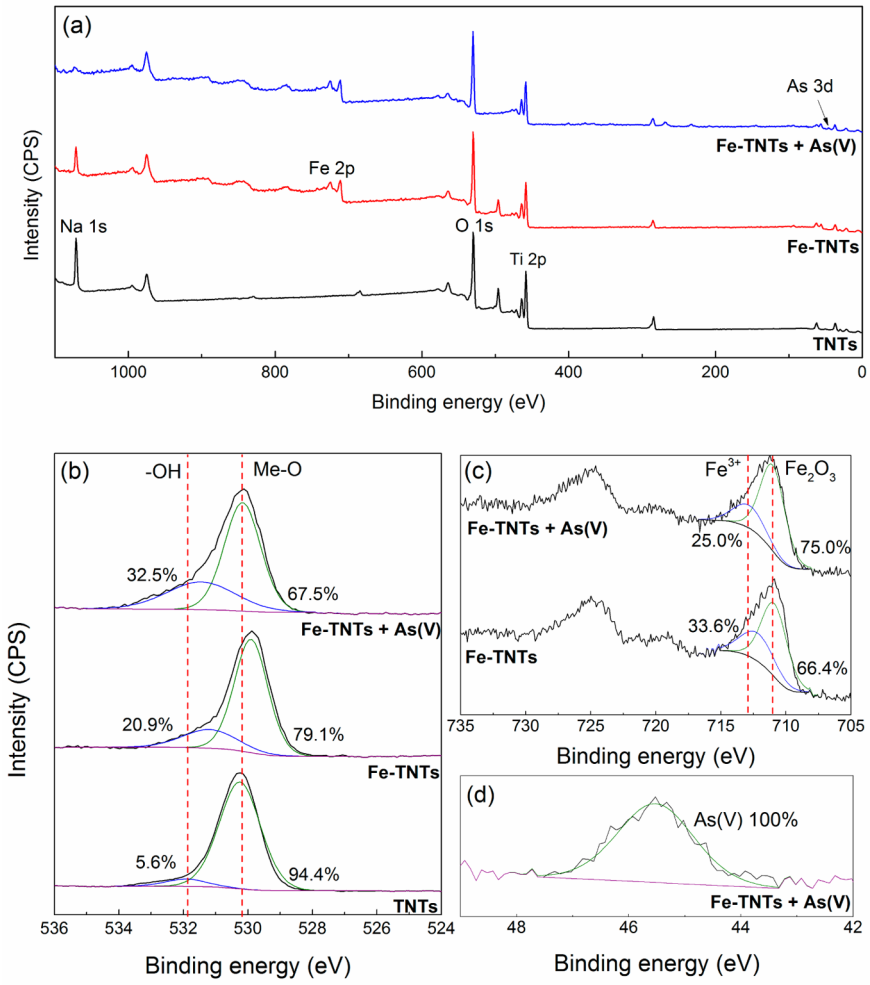

Figure 9. XPS spectra for TNTs, Fe-TNTs, and Fe-TNTs with As(V): (a) survey and high-resolution spectra of (b) O 1s, (c) Fe 2p, and (d) As 3d.

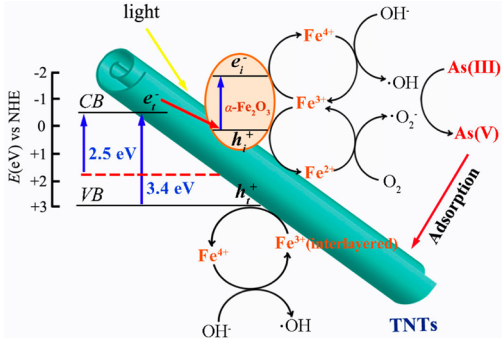

Figure 10. Schematic diagram of the photocatalysis of As(III) and adsorption of As(V) on Fe-TNTs.

dissolved into solutions from Fe-TNTs after 5 cycles, indicating the great stability of this material. Therefore, Fe-TNTs are of great potential for As removal in practical wastewaters.

4. CONCLUSIONS

Fe-deposited titanate nanotubes (Fe-TNTs) were synthesized through a one-step hydrothermal method. The as-prepared material possessed a tubular structure, with Fe_2O_3 nanoparticles attached to the tubes. XRD and XPS analyses showed that the deposited Fe existed in two forms: Fe^{3+} located in the interlayers of TNTs and α-Fe_2O_3 attached on the nanotubes.

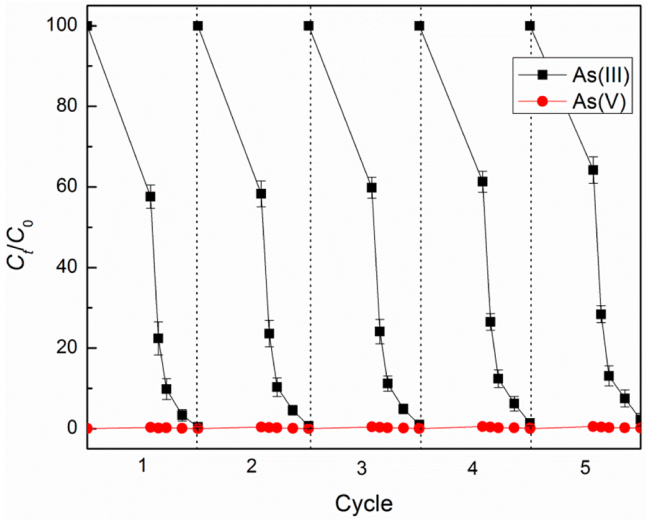

Figure 11. Reuse of Fe-TNTs for As(III) and As(V) removal over 5 photocatalysis–adsorption cycles under visible light (initial As(III) concentration = 10 mg L^{-1}; material dosage = 0.6 g L^{-1}; solution pH = 3.0).

The optimum material dosage for As(III) and As(V) removal was found to be 0.6 g L^{-1} UV under both UV and visible light. The As(III) removal efficiency reached 99.6% within 30 min for

DOI: 10.1021/acsami.5b05263
ACS Appl. Mater. Interfaces 2015, 7, 19726–19735

an initial dosage of 0.6 g L^{-1} Fe-TNTs under UV light irradiation. The apparent rate constant for photo-oxidation of As(III) by Fe-TNTs (0.1512 min^{-1}) was almost 250 times that by unmodified TNTs, indicating significant enhancement of photocatalytic activity after the Fe was deposited. In addition, As(V) was immediately adsorbed onto Fe-TNTs, and almost no As(V) could be detected throughout the entire photocatalysis−adsorption process. Excellent photocatalytic activity was also found under visible light irradiation, with 99.5% of As(III) photo-oxidized within 180 min for an initial dosage of 0.6 g L^{-1} Fe-TNTs. Dual-enhancement of photocatalytic activity occurred after Fe was deposited for the following reasons: (1) interlayered Fe^{3+} acted as a temporary electron or hole-trapping site; (2) α-Fe_2O_3 acted as a charge carrier for electron transferred from TNTs. Both led to inhibited electron−hole pair recombination. Moreover, the adsorptive performance of Fe-TNTs was also improved due to the presence of attached α-Fe_2O_3, resulting in efficient removal of As(V) through complexation. Initial photocatalysis of As(III) and subsequent adsorption of As(V) indicated the key role played by Fe used to modify TNTs. Fe is an ideal metal for TNTs modification so as to greatly enhance the photocatalytic and adsorptive property of conventional TNTs, thus achieving the goal of simultaneous removal of As(III) and As(V).

■ ASSOCIATED CONTENT

Supporting Information

The Supporting Information is available free of charge on the ACS Publications website at DOI: 10.1021/acsami.5b05263.

Figures with characterization information, details of photo-oxidations, PL spectra, kinetics plots, adsorption kinetics, isotherm, and mechanism (PDF)

■ AUTHOR INFORMATION

Corresponding Author

*E-mail: nijinren@iee.pku.edu.cn. Phone: +86-10-6275-1185. Fax: +86-10-6275-6526.

Notes

The authors declare no competing financial interest.

■ ACKNOWLEDGMENTS

Financial support from National Natural Science Foundation of China (Grant 51379010) is very much appreciated. Support from U.S. Department of the Interior Bureau of Ocean Energy Management (M12AC00013) and Collaborative Innovation Center for Regional Environmental Quality of China is also acknowledged.

■ REFERENCES

(1) Pelaez, M.; Nolan, N. T.; Pillai, S. C.; Seery, M. K.; Falaras, P.; Kontos, A. G.; Dunlop, P. S. M.; Hamilton, J. W. J.; Byrne, J. A.; O'Shea, K.; Entezari, M. H.; Dionysiou, D. D. A Review on the Visible Light Active Titanium Dioxide Photocatalysts for Environmental Applications. *Appl. Catal., B* **2012**, *125*, 331−349.

(2) Bavykin, D. V.; Friedrich, J. M.; Walsh, F. C. Protonated Titanates and TiO_2 Nanostructured Materials: Synthesis, Properties, and Applications. *Adv. Mater.* **2006**, *18*, 2807−2824.

(3) Kim, S.; Kim, M.; Hwang, S. H.; Lim, S. K. Enhancement of Photocatalytic Activity of Titania-Titanate Nanotubes by Surface Modification. *Appl. Catal., B* **2012**, *123−124*, 391−397.

(4) Liu, W.; Borthwick, A. G. L.; Li, X.; Ni, J. High Photocatalytic and Adsorptive Performance of Anatase-Covered Titanate Nanotubes Prepared by Wet Chemical Reaction. *Microporous Mesoporous Mater.* **2014**, *186*, 168−175.

(5) Weng, B.; Liu, S.; Tang, Z. R.; Xu, Y. J. One-Dimensional Nanostructure Based Materials for Versatile Photocatalytic Applications. *RSC Adv.* **2014**, *4*, 12685−12700.

(6) Liu, S.; Tang, Z. R.; Sun, Y.; Colmenares, J. C.; Xu, Y. J. One-Dimension-Based Spatially Ordered Architectures for Solar Energy Conversion. *Chem. Soc. Rev.* **2015**, *44*, 5053−5075.

(7) Liu, W.; Wang, T.; Borthwick, A. G. L.; Wang, Y.; Yin, X.; Li, X.; Ni, J. Adsorption of Pb^{2+}, Cd^{2+}, Cu^{2+} and Cr^{3+} onto Titanate Nanotubes: Competition and Effect of Inorganic Ions. *Sci. Total Environ.* **2013**, *456−457*, 171−180.

(8) Li, N.; Zhang, L.; Chen, Y.; Fang, M.; Zhang, J.; Wang, H. Highly Efficient, Irreversible and Selective Ion Exchange Property of Layered Titanate Nanostructures. *Adv. Funct. Mater.* **2012**, *22*, 835−841.

(9) Lin, C. H.; Wong, D. S. H.; Lu, S. Y. Layered Protonated Titanate Nanosheets Synthesized with a Simple One-Step, Low-Temperature, Urea-Modulated Method as an Effective Pollutant Adsorbent. *ACS Appl. Mater. Interfaces* **2014**, *6*, 16669−16678.

(10) Lee, C. K.; Wang, C. C.; Lyu, M. D.; Juang, L. C.; Liu, S. S.; Hung, S. H. Effects of Sodium Content and Calcination Temperature on the Morphology, Structure and Photocatalytic Activity of Nanotubular Titanates. *J. Colloid Interface Sci.* **2007**, *316*, 562−569.

(11) Yu, H.; Yu, J.; Cheng, B.; Zhou, M. Effects of Hydrothermal Post-Treatment on Microstructures and Morphology of Titanate Nanoribbons. *J. Solid State Chem.* **2006**, *179*, 349−354.

(12) Tang, Z. R.; Zhang, Y. H.; Xu, Y. J. Tuning the Optical Property and Photocatalytic Performance of Titanate Nanotube toward Selective Oxidation of Alcohols under Ambient Conditions. *ACS Appl. Mater. Interfaces* **2012**, *4*, 1512−1520.

(13) Bavykin, D. V.; Kulak, A. N.; Shvalagin, V. V.; Andryushina, N. S.; Stroyuk, O. L. Photocatalytic Properties of Rutile Nanoparticles Obtained via Low Temperature Route from Titanate Nanotubes. *J. Photochem. Photobiol., A* **2011**, *218*, 231−238.

(14) Yu, J.; Yu, H.; Cheng, B.; Trapalis, C. Effects of Calcination Temperature on the Microstructures and Photocatalytic Activity of Titanate Nanotubes. *J. Mol. Catal. A: Chem.* **2006**, *249*, 135−142.

(15) Chen, H. Y.; Lo, S. L.; Ou, H. H. Catalytic Hydrogenation of Nitrate on Cu-Pd Supported on Titanate Nanotube and the Experiment After Aging, Sulfide Fouling and Regeneration Procedures. *Appl. Catal., B* **2013**, *142−143*, 65−71.

(16) Grandcolas, M.; Cottineau, T.; Louvet, A.; Keller, N.; Keller, V. Solar Light-Activated Photocatalytic Degradation of Gas Phase Diethylsulfide on WO_3-Modified TiO_2 Nanotubes. *Appl. Catal., B* **2013**, *138−139*, 128−140.

(17) Gannoun, C.; Turki, A.; Kochkar, H.; Delaigle, R.; Eloy, P.; Ghorbel, A.; Gaigneaux, E. M. Elaboration and Characterization of Sulfated and Unsulfated V_2O_5/TiO_2 Nanotubes Catalysts for Chlorobenzene Total Oxidation. *Appl. Catal., B* **2014**, *147*, 58−64.

(18) Grover, I. S.; Singh, S.; Pal, B. Influence of Thermal Treatment and Au-Loading on the Growth of Versatile Crystal Phase Composition and Photocatalytic Activity of Sodium Titanate Nanotubes. *RSC Adv.* **2014**, *4*, 51342−51348.

(19) Choong, T. S. Y.; Chuah, T. G.; Robiah, Y.; Gregory Koay, F. L.; Azni, I. Arsenic Toxicity, Health Hazards and Removal Techniques from Water: An Overview. *Desalination* **2007**, *217*, 139−166.

(20) Hughes, M. F. Arsenic Toxicity and Potential Mechanisms of Action. *Toxicol. Lett.* **2002**, *133*, 1−16.

(21) Straif, K.; Benbrahim-Tallaa, L.; Baan, R.; Grosse, Y.; Secretan, B.; El Ghissassi, F.; Bouvard, V.; Guha, N.; Freeman, C.; Galichet, L.; Cogliano, V. A Review of Human Carcinogens-Part C: Metals, Arsenic, Dusts, and Fibres. *Lancet Oncol.* **2009**, *10*, 453−454.

(22) Cullen, W. R.; Reimer, K. J. Arsenic Speciation in the Environment. *Chem. Rev.* **1989**, *89*, 713−764.

(23) Manning, B. A.; Fendorf, S. E.; Bostick, B.; Suarez, D. L. Arsenic(III) Oxidation and Arsenic(V) Adsorption Reactions on Synthetic Birnessite. *Environ. Sci. Technol.* **2002**, *36*, 976−981.

(24) Zhao, Z.; Jia, Y.; Xu, L.; Zhao, S. Adsorption and Heterogeneous Oxidation of As(III) on Ferrihydrite. *Water Res.* **2011**, *45*, 6496−6504.

DOI: 10.1021/acsami.5b05263
ACS Appl. Mater. Interfaces 2015, 7, 19726−19735

(25) Cao, C. Y.; Qu, J.; Yan, W. S.; Zhu, J. F.; Wu, Z. Y.; Song, W. G. Low-Cost Synthesis of Flowerlike α-Fe_2O_3 Nanostructures for Heavy Metal Ion Removal: Adsorption Property and Mechanism. *Langmuir* **2012**, *28*, 4573−4579.
(26) Jin, Y.; Liu, F.; Tong, M.; Hou, Y. Removal of Arsenate by Cetyltrimethylammonium Bromide Modified Magnetic Nanoparticles. *J. Hazard. Mater.* **2012**, *227*−*228*, 461−468.
(27) Niu, H. Y.; Wang, J. M.; Shi, Y. L.; Cai, Y. Q.; Wei, F. S. Adsorption Behavior of Arsenic onto Protonated Titanate Nanotubes Prepared via Hydrothermal Method. *Microporous Mesoporous Mater.* **2009**, *122*, 28−35.
(28) Wang, Y.; Liu, W.; Wang, T.; Ni, J. Arsenate Adsorption onto Fe-TNTs Prepared by a Novel Water-Ethanol Hydrothermal Method: Mechanism and Synergistic Effect. *J. Colloid Interface Sci.* **2015**, *440*, 253−262.
(29) Liu, W.; Ni, J.; Yin, X. Synergy of Photocatalysis and Adsorption for Simultaneous Removal of Cr(VI) and Cr(III) with TiO_2 and Titanate Nanotubes. *Water Res.* **2014**, *53*, 12−25.
(30) Xiong, L.; Yang, Y.; Mai, J.; Sun, W.; Zhang, C.; Wei, D.; Chen, Q.; Ni, J. Adsorption Behavior of Methylene Blue onto Titanate Nanotubes. *Chem. Eng. J.* **2010**, *156*, 313−320.
(31) Chen, Q.; Peng, L. M. Structure and Applications of Titanate and Related Nanostructures. *Int. J. Nanotechnol.* **2007**, *4*, 44−65.
(32) Sun, X.; Li, Y. Synthesis and Characterization of Ion-Exchangeable Titanate Nanotubes. *Chem. - Eur. J.* **2003**, *9*, 2229−238.
(33) Chen, Q.; Zhou, W.; Du, G. H.; Peng, L. M. Trititanate Nanotubes Made via a Single Alkali Treatment. *Adv. Mater.* **2002**, *14*, 1208−1211.
(34) Xiong, L.; Chen, C.; Chen, Q.; Ni, J. Adsorption of Pb(II) and Cd(II) from Aqueous Solutions Using Titanate Nanotubes Prepared via Hydrothermal Method. *J. Hazard. Mater.* **2011**, *189*, 741−748.
(35) Wang, C. T.; Ro, S. H. Nanoparticle Iron-Titanium Oxide Aerogels. *Mater. Chem. Phys.* **2007**, *101*, 41−48.
(36) Wang, T.; Liu, W.; Xiong, L.; Xu, N.; Ni, J. Influence of pH, Ionic Strength and Humic Acid on Competitive Adsorption of Pb(II), Cd(II) and Cr(III) onto Titanate Nanotubes. *Chem. Eng. J.* **2013**, *215*−*216*, 366−374.
(37) Brunauer, S.; Deming, L. S.; Deming, W. E.; Teller, E. On a Theory of the van der Waals Adsorption of Gases. *J. Am. Chem. Soc.* **1940**, *62*, 1723−1732.
(38) Yu, J.; Yu, J. C.; Leung, M. K. P.; Ho, W.; Cheng, B.; Zhao, X.; Zhao, J. Effects of Acidic and Basic Hydrolysis Catalysts on the Photocatalytic Activity and Microstructures of Bimodal Mesoporous Titania. *J. Catal.* **2003**, *217*, 69−78.
(39) Turki, A.; Kochkar, H.; Guillard, C.; Berhault, G.; Ghorbel, A. Effect of Na Content and Thermal Treatment of Titanate Nanotubes on the Photocatalytic Degradation of Formic Acid. *Appl. Catal., B* **2013**, *138*−*139*, 401−415.
(40) Zhao, W.; Zhang, J.; Zhu, X.; Zhang, M.; Tang, J.; Tan, M.; Wang, Y. Enhanced Nitrogen Photofixation on Fe-Doped TiO_2 with Highly Exposed (101) Facets in the Presence of Ethanol as Scavenger. *Appl. Catal., B* **2014**, *144*, 468−477.
(41) Yu, J.; Xiang, Q.; Zhou, M. Preparation, Characterization and Visible-Light-Driven Photocatalytic Activity of Fe-Doped Titania Nanorods and First-Principles Study for Electronic Structures. *Appl. Catal., B* **2009**, *90*, 595−602.
(42) Zhang, F. S.; Itoh, H. Photocatalytic Oxidation and Removal of Arsenite from Water Using Slag-Iron Oxide-TiO_2 Adsorbent. *Chemosphere* **2006**, *65*, 125−131.
(43) Serpone, N.; Lawless, D.; Khairutdinov, R. Size Effects on the Photophysical Properties of Colloidal Anatase TiO_2 Particles: Size Quantization versus Direct Transitions in This Indirect Semiconductor? *J. Phys. Chem.* **1995**, *99*, 16646−16654.
(44) Ohsaki, Y.; Masaki, N.; Kitamura, T.; Wada, Y.; Okamoto, T.; Sekino, T.; Niihara, K.; Yanagida, S. Dye-Sensitized TiO_2 Nanotube Solar Cells: Fabrication and Electronic Characterization. *Phys. Chem. Chem. Phys.* **2005**, *7*, 4157−4163.
(45) Ou, H. H.; Liao, C. H.; Liou, Y. H.; Hong, J. H.; Lo, S. L. Photocatalytic Oxidation of Aqueous Ammonia over Microwave-Induced Titanate Nanotubes. *Environ. Sci. Technol.* **2008**, *42*, 4507−4512.
(46) Zhang, Y.; Yang, M.; Dou, X. M.; He, H.; Wang, D. S. Arsenate Adsorption on an Fe−Ce Bimetal Oxide Adsorbent: Role of Surface Properties. *Environ. Sci. Technol.* **2005**, *39*, 7246−7253.
(47) Dou, X.; Zhang, Y.; Zhao, B.; Wu, X.; Wu, Z.; Yang, M. Arsenate Adsorption on an Fe-Ce Bimetal Oxide Adsorbent: EXAFS Study and Surface Complexation Modeling. *Colloids Surf., A* **2011**, *379*, 109−115.
(48) D'Arcy, M.; Weiss, D.; Bluck, M.; Vilar, R. Adsorption Kinetics, Capacity and Mechanism of Arsenate and Phosphate on a Bifunctional TiO_2-Fe_2O_3 Bi-Composite. *J. Colloid Interface Sci.* **2011**, *364*, 205−212.
(49) Biesinger, M. C.; Payne, B. P.; Grosvenor, A. P.; Lau, L. W. M.; Gerson, A. R.; Smart, R. S. C. Resolving Surface Chemical States in XPS Analysis of First Row Transition Metals, Oxides and Hydroxides: Cr, Mn, Fe, Co and Ni. *Appl. Surf. Sci.* **2011**, *257*, 2717−2730.
(50) Zhao, X.; Xia, D.; Zheng, K. Fe_3O_4/Fe/Carbon Composite and Its Application as Anode Material for Lithium-Ion Batteries. *ACS Appl. Mater. Interfaces* **2012**, *4*, 1350−1356.

DOI: 10.1021/acsami.5b05263
ACS Appl. Mater. Interfaces 2015, 7, 19726−19735